Hindawi Publishing Corporation
Journal of Nanomaterials
Volume 2013, Article ID 194854, 9 pages
http://dx.doi.org/10.1155/2013/194854

Research Article

Fabrication, Characterization, and Antimicrobial Activity, Evaluation of Low Silver Concentrations in Silver-Doped Hydroxyapatite Nanoparticles

A. Costescu,[1] C. S. Ciobanu,[2] S. L. Iconaru,[1,2] R. V. Ghita,[2] C. M. Chifiriuc,[3] L. G. Marutescu,[3] and D. Predoi[2]

[1] *Faculty of Physics, University of Bucharest, 405 Atomistilor, P.O. Box MG-1, 077125 Magurele, Romania*
[2] *National Institute of Materials Physics, 105 Bis Atomistilor, P.O. Box MG 07, 077125 Magurele, Romania*
[3] *Microbiology Department, Faculty of Biology, University of Bucharest, Aleea Portocalelor 1-3, 60101 Bucharest, Romania*

Correspondence should be addressed to D. Predoi; dpredoi@gmail.com

Received 14 February 2013; Accepted 18 April 2013

Academic Editor: Suad Rashdan

The aim of this study was the evaluation of $(Ca_{10-x}Ag_x)(PO_4)_6(OH)_2$ nanoparticles (Ag:HAp-NPs) for their antibacterial and antifungal activity. Resistance to antimicrobial agents by pathogenic bacteria has emerged in the recent years as a major public health problem worldwide. In this paper, we report a comparison of the antimicrobial activity of low concentrations silver-doped hydroxyapatite nanoparticles. The silver-doped nanocrystalline hydroxyapatite powder was synthesized at 100°C in deionised water. The as-prepared Ag:Hap nanoparticles were characterized by X-ray diffraction (XRD), transmission electron microscopy (TEM), FT-IR, and FT-Raman spectroscopy. X-ray diffraction (XRD) studies demonstrate that powders obtained by coprecipitation at 100°C exhibit the apatite characteristics with good crystal structure, without any new phase or impurities found. FT-IR and FT-Raman spectroscopy revealed the presence of the various vibrational modes corresponding to phosphates and hydroxyl groups and the absence of any band characteristic to silver. The specific microbiological assays demonstrated that Ag:HAp-NPs exhibited antimicrobial features, but interacted differently with the Gram-positive, Gram-negative bacterial and fungal tested strains.

1. Introduction

Nanotechnology is at the base of recent and future developments in technological and industrial applications. In last years, the progress made in the area of engineered nanomaterials allowed us to have spectacular inside knowledge about materials at an atomic and molecular scale. Recently, biomaterials are emerging as the most studied area of materials science [1–6]. Biomaterials could be defined as "implantable materials that perform their function in contact with living tissues" [7]. This is a new interdisciplinary branch set to achieve new and improved materials with biological properties for use in clinical applications. The aim of this research direction is to study, facilitate, and improve the biological interactions between materials and organisms. The inorganic materials with good biological properties are intensively studied for this purpose. The most studied biomaterials are those based on calcium phosphate, which belongs to the so-called apatite's family. An important representative of the apatite's family is hydroxyapatite with the general formula $Ca_{10}(PO_4)_6(OH)_2$. Due to its outstanding properties such as biocompatibility, osteoconductivity, and bioactivity, the hydroxyapatite (HAp) has been extensively investigated [8, 9]. It is found naturally in the human body as one of the major constituents of bones and teeth. HAp nanoparticles have been investigated as coatings of medical implants for use in dentistry and orthopaedics as prosthesis due to their excellent properties [10]. Even though these nanoparticles have excellent biocompatibility, one of the most significant problems nowadays when using implants is the risk of infections. The development of surgical infections is common and widely spread amongst patients despite the hospitals tremendous efforts to avoid them. Due to the high costs and mortality rates, the research towards developing new

compounds with high biocompatibility and antimicrobial properties is a hot topic at global scale. Silver has been used since ancient times as an efficient antimicrobial agent, being active against a wide range of microorganisms [11]. In agreement with Clement and Jarrett [12], the understanding of silver toxicity to bacteria and of bacterial resistance mechanisms has a long way to go. Silver binds to many cellular components, the interaction with the membrane components probably being more important than that with the nucleic acids [12]. Hydroxyapatite has the ability to achieve the substitution of Ca^{2+} ions with other metal ions such as Cu^{2+}, Zn^{2+}, and Ag^{2+}, without changing its initial structure and properties.

In this paper, we report a novel compound based on low silver concentrations in silver doped hydroxyapatite nanoparticles with high biocompatibility, synthesized at low temperature using the coprecipitation method. Characterization of the Ag:Hap ($0 \le x_{Ag} \le 0.1$) using X-ray diffraction (XRD) and transmission electron microscopy (TEM) confirmed that the product consists of pure HAp ellipsometric nanoparticles. The antimicrobial properties of $(Ca_{10-x}Ag_x)(PO_4)_6(OH)_2$, with $0 \le x_{Ag} \le 0.1$ nanoparticles were evaluated on Gram-negative (*Escherichia coli* ATCC 25922, *E. coli* 714, *K. pneumoniae* 2968) and Gram-positive (*Bacillus subtilis*) bacterial strains as well as *Candida krusei* 963 yeast.

2. Experimental Section

2.1. Sample Preparation. The reagents used for the synthesis of silver doped hydroxyapatite were ammonium dihydrogen phosphate $[(NH_4)_2HPO_4]$ (Alpha Aesare, Germany, 99.99% purity), calcium nitrate $[Ca(NO_3)_2{\cdot}4H_2O]$ (Alpha Aesare, Germany, 99.99% purity), silver nitrate $AgNO_3$ (Alpha Aesare, Germany, 99.99% purity), and ammonium hydroxide NH_4OH (Alpha Aesare, Germany, 99.99% purity).

The synthesis of $(Ca_{10-x}Ag_x)(PO_4)_6(OH)_2$, with $x_{Ag} = 0$, $x_{Ag} = 0.02$, $x_{Ag} = 0.05$, $x_{Ag} = 0.07$, and $x_{Ag} = 0.1$ was carried out as reported [13, 14]. The synthesis of Ag:HAp with $x_{Ag} = 0$ was carried out as reported [13, 14] by the following reaction [15]:

$$10Ca(NO_3)_2{\cdot}4H_2O + 6(NH_4)_2HPO_4 + 2NH_4OH \longrightarrow Ca_{10}(PO_4)_6(OH)_2 + 20NH_4NO_3 + 46H_2O \quad (1)$$

The pH of solution was adjusted to 10 with ammonium hydroxide (NH_4OH) in accord with [16]. Nanocrystalline hydroxyapatite doped with Ag was performed by setting the x_{Ag} from 0 to 0.1 ($0 \le x_{Ag} \le 0.1$) and [Ca+Ag]/P as 1.67. The $AgNO_3$ and $Ca(NO_3)_2{\cdot}4H_2O$ were dissolved in deionised water to obtain 300 mL [Ca+Ag]-containing solution. On the other hand, the $(NH_4)_2HPO_4$ was dissolved in deionised water to make 300 mL P-containing solution. The [Ca+Ag]-containing solution was stirred at 100°C for 30 minutes. Meanwhile the pH of P-containing solution was adjusted to 10 with ammonium hydroxide (NH_4OH) and stirred continuously for 30 minutes. The P-containing solution was added drop by drop into the [Ca+Ag]-containing solution and stirred for 2 h and the pH was constantly adjusted and kept at 10 during the reaction. When the reaction was complete, the deposited mixtures were washed several times with deionised water. The resulting material (Ag:HAp) was dried at 100°C for 72 h.

Silver doped hydroxyapatite powders (Ag:HAp) with $x_{Ag} \neq 0$, setting the x_{Ag} from 0.02 to 0.1 ($0.02 \le x_{Ag} \le 0.1$), were prepared assuming that silver ions would substitute for the calcium site in the HAp lattice.

According to Nath et al. [17], it is important to note that the acceptable reason for this phenomenon is that the radius of silver ion is bigger than that of the strontium ion (11.5%) with fewer valence electrons. It is also important to note that Ma et al. [18] and Corami et al. [19] in two separate research studies suggested some reactions for ion exchange between heavy metals and apatite particles.

The diffusion of Ag in HAp lattice can be characterized by the following equation [17]:

$$Ca_{10}(PO_4)_6(OH)_2 + 2xAg \xrightarrow{O} 2Ca_{10-x}Ag_{2x}(PO_4)_6(OH)_2 + xCaO \quad (2)$$

This equation indicates that Ag can be incorporated into the lattice of HAp, which is schematically shown by [17]. According to Nath et al., the complex crystal structure of HAp is described by Ca triangle around the OH column. It is worth mentioning that, in the presence of Ag, one of the Ca^{2+} sites can be substituted by Ag. Nath et al. also confirmed this substitution mechanism using Raman spectroscopy by confirming the presence of Ag–O bond. Nath et al. [17] and Nazari et al. [20] showed that because of valency difference between Ca and Ag ions, a vacancy will be created in the anion site, as per the following defect reaction:

$$2Ag \xrightarrow{Ca^{2+}} 2Ag'_{Ca} + V_O^{\infty} \quad (3)$$

As shown by Nath et al. and Nazari et al., it can be perceived that the creation of oxygen vacancy will enable the proton of OH-bond to be attracted towards Ag-defect in the HAp structure.

2.2. Sample Characterization. The X-ray diffraction measurements for the Ag:HAp samples were recorded using a Bruker D8 Advance diffractometer, with nickel filtered Cu K_α ($\lambda = 1.5418$ Å) radiation with a high efficiency one-dimensional detector (Lynx Eye type) operated in integration mode. The diffraction patterns were collected in the 2θ range 20°–70°, with a step of 0.02° and 34 s measuring time per step. Transmission electron microscopy (TEM) studies were carried out using a FEI Tecnai 12 equipped with a low dose Gatan digital camera. The specimen for TEM imaging was prepared by ultra microtomy in order to obtain thin section of about 60 nm. The powder was embedded in an epoxy resin (polaron 612) before microtomy. TEM modes used were bright field (BF) and selected area diffraction (SAD). The functional groups present in the prepared nanoparticles and thin films were identified by FTIR using a Spectrum BX spectrometer. In order to obtain the nanoparticles spectra,

1% of the nanopowder was mixed and ground with 99% KBr. Tablets of 10 mm diameter were prepared by pressing the powder mixture at a load of 5 tons for 2 min. The spectrum was recorded in the range of 500 to 4000 cm^{-1} with 4 cm^{-1} resolution. Micro-Raman spectra on powders were performed in a backscattering geometry at room temperature and in ambient air, under a laser excitation wavelength of 514 nm, using a Jobin Yvon T64000 Raman spectrophotometer under a microscope. Chemical analyses of samples were performed by HITACHI Z-8100 Polarized Zeeman Atomic Spectrophotometer performed at the Fonctionnement et Evolution des Biogéosystèmes Continentaux (Institut des Sciences de la Terre d' Orléans, France).

For the antimicrobial assays, microbial suspensions of 1.5×10^8 CFU/mL corresponding to 0.5 McFarland density obtained from 15 to 18 h bacterial cultures developed on solid media were used. The tested substances were solubilised in DMSO and the starting stock solution was of 5000 μg/mL concentration. The quantitative assay was performed by liquid microdilution method [21–27].

3. Results and Discussions

Figure 1 shows the XRD patterns of pure HAp ($x_{Ag} = 0$), Ag:HAp ($x_{Ag} = 0.02$, $x_{Ag} = 0.05$, $x_{Ag} = 0.07$, and $x_{Ag} = 0.1$) and the standard data for the hexagonal hydroxyapatite. For pure HAp ($x_{Ag} = 0$) and Ag:HAp ($x_{Ag} = 0.02$, $x_{Ag} = 0.05$, $x_{Ag} = 0.07$, and $x_{Ag} = 0.1$), the diffraction peaks can be well indexed to the hexagonal $Ca_{10}(PO_4)_6(OH)_2$ in $P6_3m$ space group (ICDD-PDF No. 9-432). The XRD analysis of Ag:HAp nanoparticles did not give the characteristic peak for silver or other phases. The XRD patterns of HAp and Ag:HAp also demonstrate that powders made by coprecipitation at 100°C with low silver concentrations in silver doped hydroxyapatite nanoparticles exhibit the apatite characteristics with good crystal structure and no new phase or impurity is found in good accord with our previous studies [13, 14, 28, 29].

The absence of other phases in XRD pattern of Ag:HAp samples demonstrates that the Ag^+ ions have successfully substituted Ca^{2+} ions without affecting the crystal structure of the original HAp. This result is in agreement with previous studies conducted by Ravindran et al., in 2010 [29], and Shirkhanzadeh et al., in 1995 [30].

The morphology and particle size of nanopowders were determined by TEM observation. Figure 2 shows TEM images of Ag:HAp ($x_{Ag} = 0$). As shown in Figure 1, Ag:HAp nanoparticles exhibited an ellipsoidal morphology which is consistent with the SEM results [13].

Figure 3 exhibits the TEM images of Ag:HAp ($x_{Ag} = 0.02$, $x_{Ag} = 0.05$, $x_{Ag} = 0.07$, and $x_{Ag} = 0.1$) at low resolution. No obvious morphological changes are observed between the initial HAp and the corresponding Ag:HAp ($x_{Ag} = 0.02$, $x_{Ag} = 0.05$, $x_{Ag} = 0.07$, and $x_{Ag} = 0.1$), and new fine particles were formed. The Ag:HAp nanoparticles preserve the morphology of pure HAp prepared by coprecipitation method [14, 28]. The long axis corresponded to the c-axis of the hexagonal HAp structure.

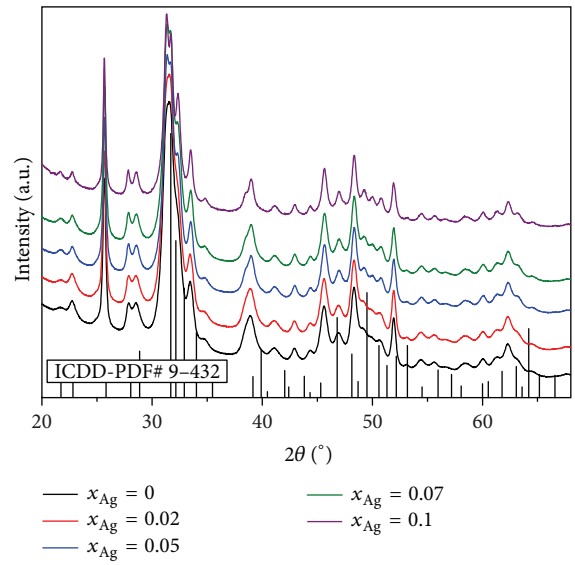

Figure 1: Comparative representation of the experimental XRD patterns of the Ag:HAp samples synthesized $x_{Ag} = 0$, $x_{Ag} = 0.02$, $x_{Ag} = 0.05$, $x_{Ag} = 0.07$, and $x_{Ag} = 0.1$, and the characteristic lines of hydroxyapatite according to the ICDD-PDF number 9-432.

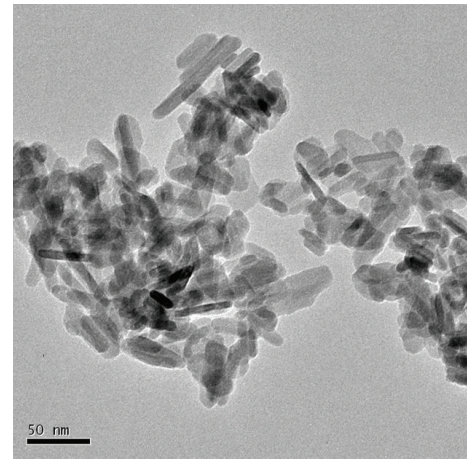

Figure 2: The TEM images of Ag:HAp ($x_{Ag} = 0$) at low resolution.

It can be seen from the HRTEM image of Ag:HAp (Figure 4(a)) the crystalline phase of hydroxyapatite with well-resolved lattice fringes. The distances between the adjacent lattice fringes (2.81 Å and 1.94 Å) agree well with the d_{211} and d_{222} spacing values from the literature (ICDD-PDF no. 9-432). All the samples exhibit a uniform ellipsoidal morphology with particles from 5 nm to 15 nm. Figure 4(b) shows a selected area electron diffraction (SAED) pattern recorded from an area containing a large number of ellipsometric nanoparticles. The rings in the SAED pattern can be indexed as (002), (210), (211), (310), (222), (213), (004), and (304) reflections of the hexagonal HAp, in agreement with the XRD results. No extra reflections are observed and we can therefore conclude that the product consists of pure HAp ellipsometric nanoparticles.

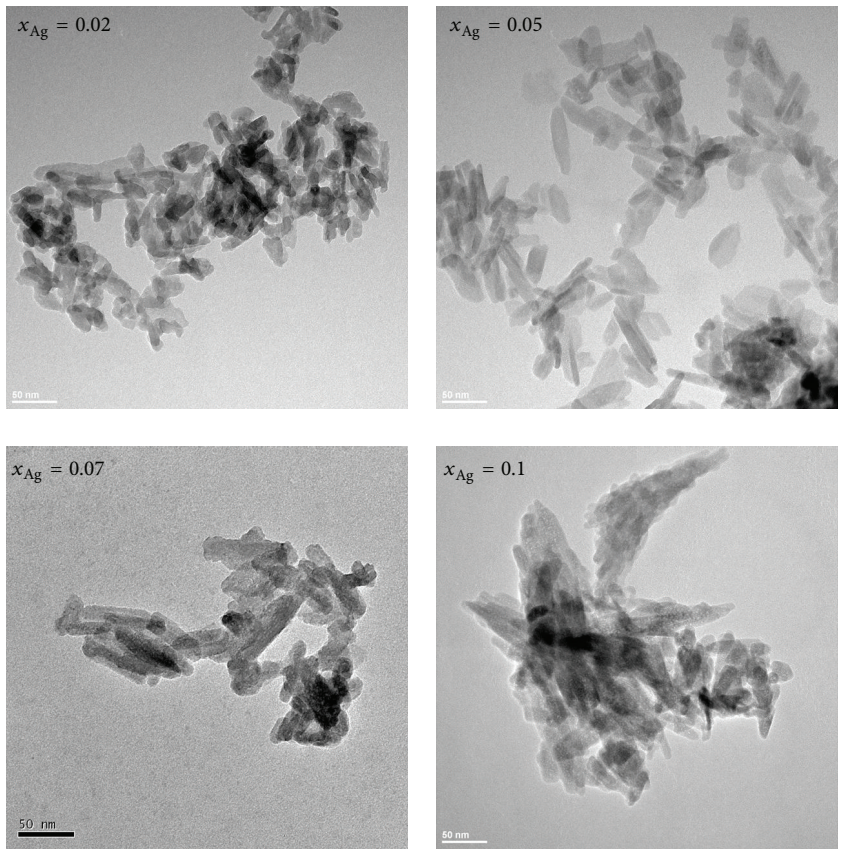

Figure 3: The TEM images of Ag:HAp (x_{Ag} = 0.02, x_{Ag} = 0.05, x_{Ag} = 0.07, and x_{Ag} = 0.1) at low resolution.

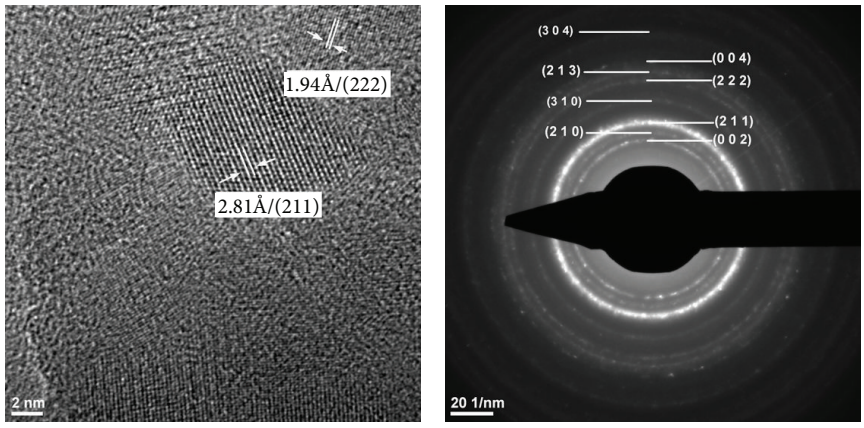

(a) (b)

Figure 4: HRTEM image and SAED analysis of Ag:HAp with x_{Ag} = 0.05.

These results are well consistent with the XRD results revealing that the doping components have little influence on the surface morphology of the samples. The morphology identifications indicated that the nanoparticles with good crystal structure could be made by coprecipitation method at low temperature.

FT-IR spectroscopy was performed in order to investigate the functional groups present in nanohydroxyapatite, $Ca_{10-x}Ag_x(PO_4)_6(OH)_2$, ($x_{Ag}$ = 0, x_{Ag} = 0.02, x_{Ag} = 0.05, x_{Ag} = 0.07, and x_{Ag} = 0.1) synthesized at 100°C by coprecipitation method. Figure 5 shows the FT-IR results obtained from Ag:HAp-NPs when the x_{Ag} increases from 0.05 to 0.3. The absorption peak in the region of 1600–1700 cm^{-1} ascribed to O–H bending mode is evidence of the presence of absorbed water in the synthesized products [31, 32].

The data clearly reveals the presence of various vibrational modes corresponding to phosphate and hydroxyl groups. For all the samples, the presence of strong OH vibration

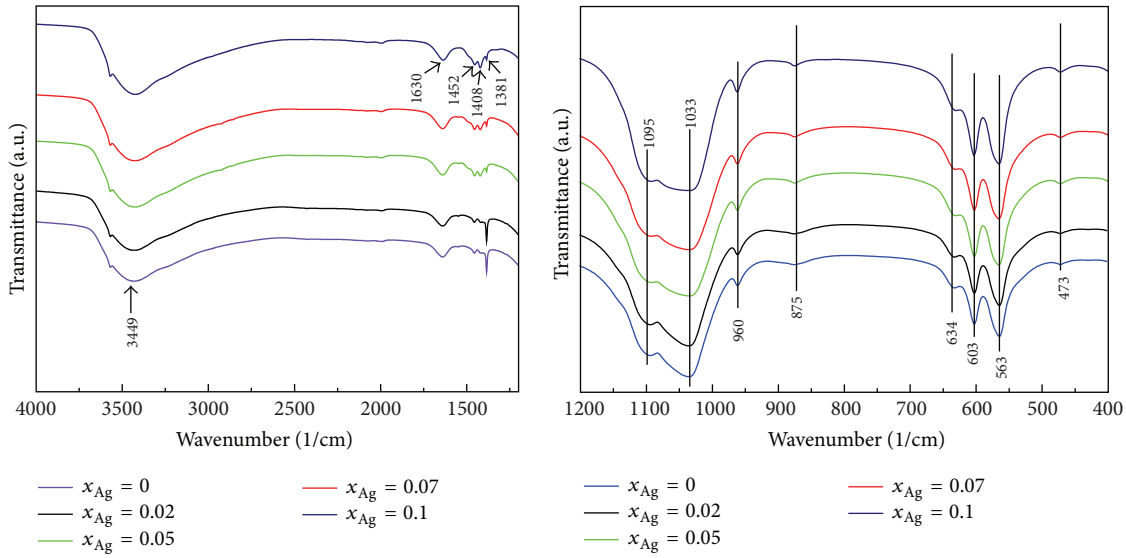

FIGURE 5: Transmittance infrared spectra of the Ag:HAp samples synthesized with $x_{Ag} = 0$, $x_{Ag} = 0.02$, $x_{Ag} = 0.05$, $x_{Ag} = 0.07$, and $x_{Ag} = 0.1$.

peak could be noticed. The peak observed at 634 cm^{-1} is attributed to the characteristic stretching and vibrational modes of structural OH groups [33]. The band at 1630 cm^{-1} corresponds to the adsorbed H_2O [33]. The broad bands in the regions 1600–1700 cm^{-1} and 3200–3600 cm^{-1} correspond to H–O–H bands of water lattice [34].

Bands characteristics of PO_4^{3-} tetrahedral apatite's structure are clearly observed at 473 cm^{-1}, 563 cm^{-1}, 603 cm^{-1}, 960 cm^{-1}, and 1095–1033 cm^{-1} [35, 36]. The peak at 473 cm^{-1} is attributed to PO_4 ν_2. The peaks at 563 cm^{-1} and 603 cm^{-1} belong to PO_4 ν_4. The peak at 960 cm^{-1} is attributed to PO_4 ν_1 and the peaks at 1095–1033 cm^{-1}, to PO_4 ν_3. A CO_3^{2-} band occurred in the spectra at 1452 and 1400 cm^{-1}. The bands at 875 cm^{-1} are attributed to HPO_4^{2-} ions [37, 38].

Complementary information can be obtained from Raman spectroscopy. Raman spectra of Ag:HAp from 1200 cm^{-1} to 400 cm^{-1} is shown in Figure 6. The OH^- vibrational bands expected in the region of 630 cm^{-1} are not clearly detected. This behavior is in good accord with the previous studies [39].

We assigned the bands present at 1026 cm^{-1} (ν_3), 1047 cm^{-1} (ν_3), and 1074 cm^{-1} (ν_3) to the asymmetric ν_3 (P–O) stretching. The internal modes of the PO_4^{3-} tetrahedral ν_1 frequency (960 cm^{-1}) correspond to the symmetric stretching of P–O bonds. The 616 cm^{-1}, 590 cm^{-1}, and 576 cm^{-1} bands arise from ν_4 PO_4 [37]. The vibrational bands at 429 cm^{-1} (ν_2) and 449 cm^{-1} (ν_2) are attributed to the O–P–O bending modes. The band at 1070 cm^{-1} (ν_1) attributed to CO_3^{2-} impurity was obscured by the intensity of PO_4 band at 1074 cm^{-1}. The other CO_3 modes ν_3, ν_4, and ν_2 have band positions not obscured by the PO_4 bands, but they have weak intensities and were not detected [40]. Water vibrational modes give rise to weak intensity stretching and bending bands in Raman spectra. These water bands,

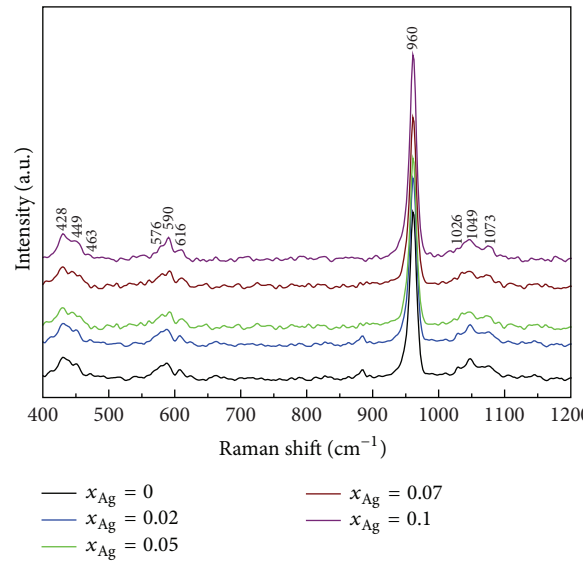

FIGURE 6: Raman spectra of the Ag:HAp samples synthesized with $x_{Ag} = 0$, $x_{Ag} = 0.02$, $x_{Ag} = 0.05$, $x_{Ag} = 0.07$, and $x_{Ag} = 0.1$.

expected at about the same wave number in FTIR spectra, were not observed in Raman spectra.

The results on chemical analyses of samples are reported in Table 1. The synthesis allowed a good control over the chemical composition of Ag:HAp powders ($x_{Ag} = 0$, $x_{Ag} = 0.02$, $x_{Ag} = 0.05$, $x_{Ag} = 0.07$, and $x_{Ag} = 0.1$), with the Ca/P and (Ca+Ag)/P atomic ratios being close to the stoichiometric value of 1.67.

The antimicrobial activity of Ag:HAp ($0 \leq x_{Ag} \leq 0.1$) nanoparticles was tested using strains belonging to the most commonly encountered pathogens: *E. coli ATCC* 25922, *E. coli* 714, *K. pneumoniae* 2968, *B. subtilis*, and *C. krusei* 963.

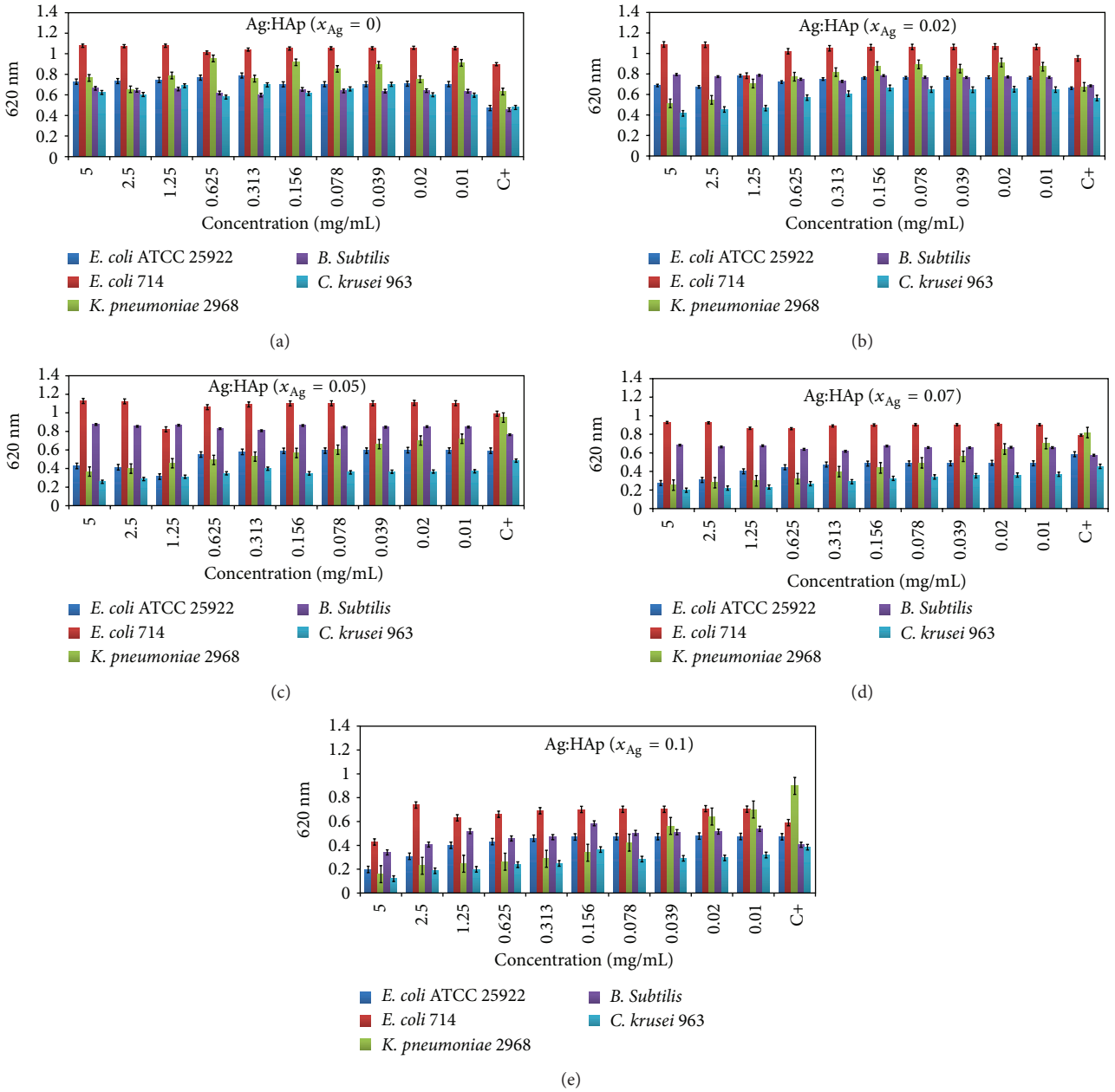

FIGURE 7: Antibacterial activity of Ag:HAp-NPs (x_{Ag} = 0, 0.02, 0.05, 0.07, and 0.1) on *E. coli* ATCC 25922, *E. coli* 714, *K. pneumoniae* 2968, *B. subtilis*, and *C. krusei* strains.

The results of microbiological assays of Ag:HAp ($0 \leq x_{Ag} \leq 0.1$) nanoparticles are shown in Figures 7(a)–7(e). The Ag:HAp ($x_{Ag} = 0$) nanoparticles exhibited no inhibitory effect on the microbial growth as compared to the positive growth control (C+) (Figure 7(a)). The Ag:HAp nanoparticles with $x_{Ag} = 0.02$ exhibited an inhibitory effect on the growth of *K. pneumoniae* at the first two tested concentrations and of *C. krusei* 963 at the first three tested concentrations (Figure 7(b)). The Ag:HAp nanoparticles with higher concentrations of Ag (x_{Ag} = 0.05; 0.07 and 0.1) showed an improved antimicrobial activity against the same two pathogens, that is, *K. pneumoniae* and *C. krusei,* but maintained for the entire range of the tested concentrations, from 5 to 0.01 mg/mL (Figures 7(c), 7(d), and 7(e)). Starting with the x_{Ag} = 0.05, the tested nanoparticles started to exhibit also an inhibitory effect against one of the two *E. coli* tested strains, that is, *E. coli* ATCC 25922, which is totally susceptible to antibiotics, being recommended as a reference strain for performing susceptibility testing. In exchange, the second *E. coli* 714 strain, which is a clinical strain, resistant to beta-lactam antibiotics, proved to be resistant to almost all tested nanoparticles, irrespective to the silver ions concentration, except the Ag:HAp nanoparticles doped x_{Ag} = 0.1, demonstrating that a potential cross-resistance mechanism could be responsible

Table 1: Chemical analyses of samples.

Samples	Ca/P (molar ratio)	Ag (%)	(Ca+Ag)/P (molar ratio)
$x_{Ag} = 0$	1.668	—	—
$x_{Ag} = 0.02$	1.673	1.89	1.675
$x_{Ag} = 0.05$	1.668	4.91	1.673
$x_{Ag} = 0.07$	1.666	6.97	1.669
$x_{Ag} = 0.1$	1.665	9.98	1.667

for the concomitant resistance to antibiotics and silver ions in this strain. As for *B. subtilis* strain, only the nanoparticles doped with the highest concentration of silver exhibited an inhibitory effect. These results are clearly demonstrating that the antimicrobial effect of the silver doped nanoparticles is dependent on the structure of the microbial cell wall.

Kreibig and Vollmer [40], Morones et al. [41], and Pal et al. [42] demonstrated that the nanosize of the nanoparticles assures a large surface contact area with the microbial cells and, hence, a better interaction with the microbial target will occur. Raimondi et al. [43] and Bai et al. [36], studying the inhibition of bacterial growth by differentially shaped nanoparticles, showed that the antibacterial efficacy of the nanoparticles depends on the shape of nanoparticles. In their studies, Pal et al. [42] show that, in the case of spherical nanoparticles, total silver content of 12.5 μg is needed while the rod shaped particles need a total of 50 to 100 μg of silver content. Our study demonstrates that the antibacterial activity of Ag:HAp nanoparticles is dependent on the silver concentration, with the intensity of the inhibitory effect increasing proportionally from 0.01 mg/mL to 5 mg/mL. In order to obtain a large and effective antimicrobial spectrum, including the Gram-negative, Gram-positive bacterial and fungal strains, a higher Ag:Hap concentration of 5 mg/mL is required for this type of nanoparticles. However, further studies are needed to evaluate the cytotoxicity of the nanoparticles doped with this silver concentration, before recommending them for *in vivo* clinical applications.

4. Conclusions

The Ag:HAp nanoparticles obtained by coprecipitation method at low temperature have good crystal structure and doping components have little influence on the surface morphology of the samples. The DRX analysis of Ag:Hap did not exhibit the characteristic peak for silver. Low silver concentrations are required to be effective against Gram-negative bacterial and fungal strains, but, however, the intensity of the antimicrobial effect against these strains is increasing with the silver ions concentration. Only high Ag:HAp concentration of 5 mg/mL was effective against the Gram-positive bacterial strains. The antimicrobial properties of Ag:HAp nanoparticles are supporting their potential use for various medical applications, for example, textile dressings, orthopedic and dental prostheses, or implants with improved resistance to microbial colonization.

Acknowledgments

The financial and encouragement support was provided by the Ministry of Education of Romania, project no: C2-06 under program CEA-IFA, Programul Nucleu PN 45, program 94/PN2/PCCA (2012–2014) (AntiBioTube). The authors gratefully acknowledge the support given to this work by Dr. F. Massuyeau from the Institut des Matériaux-Jean Rouxel, France.

References

[1] M. Vallet-Regí, "Evolution of bioceramics within the field of biomaterials," *Comptes Rendus Chimie*, vol. 13, no. 1-2, pp. 174–185, 2010.

[2] Z. Shi, X. Huang, Y. Cai, R. Tang, and D. Yang, "Size effect of hydroxyapatite nanoparticles on proliferation and apoptosis of osteoblast-like cells," *Acta Biomaterialia*, vol. 5, no. 1, pp. 338–345, 2009.

[3] J. Baier, R. Strumberger, F. Berger, P. Atanasova, U. Welzel, and J. Bill, "Mineralization and particle growth kinetics of ZnO in the presence of gelatin," *Biointerface Research in Applied Chemistry*, vol. 2, no. 3, pp. 339–349, 2012.

[4] J. Baier, T. Naumburg, N. J. Blumenstein et al., "Bio-inspired mineralization of zinc oxide in presence of ZnO-binding peptides," *Biointerface Research in Applied Chemistry*, vol. 2, no. 3, pp. 380–391, 2012.

[5] A. M. Grumezescu, E. Andronescu, A. Ficai, C. Bleotu, and M. C. Chifiriuc, "Chitin based biomaterial for antimicrobial therapy: fabrication, characterization and in vitro profile based interaction with eukaryotic and prokaryotic cells," *Biointerface Research in Applied Chemistry*, vol. 2, no. 5, pp. 438–445, 2012.

[6] A. M. Grumezescu, E. Andronescu, A. Ficai et al., "Water soluble magnetic biocomposite with pontetial applications for the antimicrobial therapy," *Biointerface Research in Applied Chemistry*, vol. 2, no. 6, pp. 469–475, 2012.

[7] C. S. Ciobanu, S. L. Iconaru, E. Gyorgy et al., "Biomedical properties and preparation of iron oxide-dextran nanostructures by maple technique," *Chemistry Central Journal*, vol. 6, article 17, 2012.

[8] S. L. Iconaru, E. Andronescu, C. S. Ciobanu, A. M. Prodan, P. Le Coustumer, and D. Predoi, "Biocompatible magnetic iron oxide nanoparticles doped dextran thin films produced by spin coating deposition solution," *Digest Journal of Nanomaterials and Biostructures*, vol. 7, no. 1, pp. 399–409, 2012.

[9] S. L. Iconaru, A. M. Prodan, P. Le Coustumer, and D. Predoi, "Synthesis, antibacterial and antibiofilm activity of iron oxide glycerol nanoparticles obtained by co-precipitation method," *Journal of Chemistry*, vol. 2013, Article ID 412079, 6 pages, 2013.

[10] Habraken WJEM, J. G. C. Wolke, and J. A. Jansen, "Ceramic composites as matrices and scaffolds fordrug delivery in tissue engineering," *Advanced Drug Delivery Reviews*, vol. 59, article 234, 2007.

[11] A. D. Russell and W. B. Hugo, "7 antimicrobial activity and action of silver," *Progress in Medicinal Chemistry*, vol. 31, pp. 351–370, 1994.

[12] J. L. Clement and P. S. Jarrett, "Antibacterial silver," *Metal-Based Drugs*, vol. 1, article 467, 1994.

[13] C. S. Ciobanu, F. Massuyeau, L. V. Constantin, and D. Predoi, "Structural and physical properties of antibacterial Ag-doped nano-hydroxyapatite synthesized at 100°C," *Nanoscale Research Letters*, vol. 6, article 613, 2011.

[14] C. S. Ciobanu, S. L. Iconaru, P. Le Coustumer, L. V. Constantin, and D. Predoi, "Antibacterial activity of silver-doped hydroxyapatite nanoparticles against gram-positive and gram-negative bacteria," *Nanoscale Research Letters*, vol. 7, article 324, 2012.

[15] I. Cacciotti, A. Bianco, M. Lombardi, and L. Montanaro, "Mg-substituted hydroxyapatite nanopowders: synthesis, thermal stability and sintering behaviour," *Journal of the European Ceramic Society*, vol. 29, no. 14, pp. 2969–2978, 2009.

[16] A. Bianco, I. Cacciotti, M. Lombardi, L. Montanaro, and G. Gusmano, "Thermal stability and sintering behaviour of hydroxyapatite nanopowders," *Journal of Thermal Analysis and Calorimetry*, vol. 88, no. 1, pp. 237–243, 2007.

[17] S. Nath, S. Kalmodia, and B. Basu, "Densification, phase stability and in vitro biocompatibility property of hydroxyapatite-10 wt% silver composites," *Journal of Materials Science: Materials in Medicine*, vol. 21, no. 4, pp. 1273–1287, 2010.

[18] Q. Y. Ma, S. J. Tralna, T. J. Logan, and J. A. Ryan, "Effects of aqueous AI, Cd, Cu, Fe(II), Ni, and Zn on Pb immobilization by hydroxyapatite," *Environmental Science and Technology*, vol. 28, no. 7, pp. 1219–1228, 1994.

[19] A. Corami, S. Mignardi, and V. Ferrini, "Cadmium removal from single- and multi-metal (Cd + Pb + Zn + Cu) solutions by sorption on hydroxyapatite," *Journal of Colloid and Interface Science*, vol. 317, no. 2, pp. 402–408, 2008.

[20] A. G. Nazari, A. Tahari, F. Moztarzadeh, M. Mozafari, and M. E. Bahrololoom, "Ion exchange behaviour of silver-doped apatite micro- and nanoparticles as antibacterial biomaterial," *Micro and Nano Letters*, vol. 6, no. 8, pp. 713–717, 2011.

[21] M. C. Chifiriuc, R. Palade, and A. M. Israil, "Comparative analysis of disk diffusion and liquid medium microdillution methods fortesting the antibiotic susceptibility patterns of anaerobic bacterial strains isolated from intrabdominal infections," *Biointerface Research in Applied Chemistry*, vol. 1, no. 6, pp. 209–220, 2011.

[22] P. B. Mohite, R. B. Pandhare, and S. G. Khanage, "Synthesis, characterization and antimicrobial activity of some new pyrimidines containing tetrazole," vol. 1, pp. 258–263, 2012.

[23] L. Marutescu, C. Limban, M. C. Chifiriuc, A. V. Missir, I. C. Chirita, and M. T. Caproiu, "Studies on the antimicrobial activity of new compounds containing thiourea function," *Biointerface Research in Applied Chemistry*, vol. 1, no. 6, article 236, 2011.

[24] S. G. Khanage, P. B. Mohite, R. B. Pandhare, and S. Raju, "Investigation of pyrazole and tetrazole derivatives containing 3,5 disubstituted-4H-1,2,4-triazole as a potential antitubercular and antifungal agent," *Biointerface Research in Applied Chemistry*, vol. 2, no. 2, pp. 277–283, 2012.

[25] A. P. Mishra, H. Purwar, and R. K. Jain, "Microwave synthesis, spectral, thermal and antimicrobial activities of Co(II), Ni(II) and Cu (II) metal complexes with Schiff base ligand," *Biointerface Research in Applied Chemistry*, vol. 2, no. 2, pp. 291–299, 2012.

[26] S. G. Khanage, P. B. Mohite, R. B. Pandhare, and S. A. Raju, "Synthesis, characterization and antimicrobial evaluation of 3,5 diphenyl-1H-1,2,4-triazole containing pyrazole function," *Biointerface Research in Applied Chemistry*, vol. 2, no. 3, pp. 313–319, 2012.

[27] A. I. Shah and D. S. Raj, "Design, synthesis and in vitro evaluation of the antibacterial and antifungal activity of some new dihydropyrano[3,2-c]chromene derivatives," *Biointerface Research in Applied Chemistry*, vol. 2, no. 3, pp. 320–331, 2012.

[28] C. S. Ciobanu, S. L. Iconaru, M. C. Chifiriuc, A. Costescu, P. Le Coustumer, and D. Predoi, "Synthesis and antimicrobial activity of silver-doped hydroxyapatite nanoparticles," *BioMed Research International*, vol. 2013, Article ID 916218, 10 pages, 2013.

[29] A. Ravindran, A. Singh, A. M. Raichur, N. Chandrasekaran, and A. Mukherjee, "Studies on interaction of colloidal Ag nanoparticles with bovine serum albumin (BSA)," *Colloids and Surfaces B*, vol. 76, no. 1, pp. 32–37, 2010.

[30] M. Shirkhanzadeh, M. Azadegan, and G. Q. Liu, "Bioactive delivery systems for the slow release of antibiotics: incorporation of Ag^+ ions into micro-porous hydroxyapatite coatings," *Materials Letters*, vol. 24, no. 1–3, pp. 7–12, 1995.

[31] D. Predoi, R. V. Ghita, F. Ungureanu, C. C. Negrila, R. A. Vatasescu-Balcan, and M. Costache, "Characteristics of hydroxyapatite thin films," *Journal of Optoelectronics and Advanced Materials*, vol. 9, no. 12, pp. 3827–3831, 2007.

[32] D. Predoi, M. Barsan, E. Andronescu, R. A. Vatasescu-Balcan, and M. Costache, "Hydroxyapatite-iron oxide bioceramic prepared using nano-size powders," *Journal of Optoelectronics and Advanced Materials*, vol. 9, no. 11, pp. 3609–3613, 2007.

[33] J. Qian, Y. Kang, W. Zhang, and Z. Li, "Fabrication, chemical composition change and phase evolution of biomorphic hydroxyapatite," *Journal of Materials Science: Materials in Medicine*, vol. 19, no. 11, pp. 3373–3383, 2008.

[34] C. S. Ciobanu, S. L. Iconaru, F. Massuyeau, L. V. Constantin, and D. Predoi, "Synthesis, structure, and luminescent properties of europium-doped hydroxyapatite nanocrystalline powders," *Journal of Nanomaterials*, vol. 2012, Article ID 942801, 9 pages, 2012.

[35] C. S. Ciobanu, S. L. Iconaru, P. Le Coustumer, and D. Predoi, "Vibrational investigations of silver-doped hydroxyapatite with antibacterial properties," *Journal of Spectroscopy*, vol. 2013, Article ID 471061, 5 pages, 2013.

[36] X. Bai, K. More, C. M. Rouleau, and A. Rabiei, "Functionally graded hydroxyapatite coatings doped with antibacterial components," *Acta Biomaterialia*, vol. 6, no. 6, pp. 2264–2273, 2010.

[37] A. Mortier, J. Lemaitre, and P. G. Rouxhet, "Temperature-programmed characterization of synthetic calcium-deficient phosphate apatites," *Thermochimica Acta*, vol. 143, pp. 265–282, 1989.

[38] S. Koutsopoulos, "Preparation of calcium aluminate cement for hard tissue repair: effects of lithium fluoride and maleic acid on setting behavior, compressive strength, and biocompatibility," *Journal of Biomedical Materials Research*, vol. 62, no. 4, pp. 593–599, 2002.

[39] B. O. Fowler, "Infrared studies of apatites. I. Vibrational assignments for calcium, strontium, and barium hydroxyapatites utilizing isotopic substitution," *Inorganic Chemistry*, vol. 13, no. 1, pp. 194–207, 1974.

[40] U. Kreibig and M. Vollmer, *Optical Properties of Metal Clusters*, Springer, Berlin, Germany, 1995.

[41] J. R. Morones, J. L. Elechiguerra, A. Camacho et al., "The bactericidal effect of silver nanoparticles," *Nanotechnology*, vol. 16, no. 10, pp. 2346–2353, 2005.

[42] S. Pal, Y. K. Tak, and J. M. Song, "Does the antibacterial activity of silver nanoparticles depend on the shape of the nanoparticle? A study of the gram-negative bacterium *Escherichia coli*," *Applied and Environmental Microbiology*, vol. 73, no. 6, pp. 1712–1720, 2007.

[43] F. Raimondi, G. G. Scherer, R. Kötz, and A. Wokaun, "Nanoparticles in energy technology: examples from electrochemistry and catalysis," *Angewandte Chemie—International Edition*, vol. 44, no. 15, pp. 2190–2209, 2005.